International Journal of Heat and Technology
Vol. 43, No. 3, June, 2025, pp. 997-1005
Journal homepage: http://iieta.org/journals/ijht

Heat Source Effect on Three-Dimensional Couple Stress Casson Fluid Flow via Bidirectional Stretching Surface with Chemical Reaction

Dandu Udaya Kumar*, Nainaru Tarakaramu

Department of Mathematics, School of Liberal Arts and Sciences, Mohan Babu University, Tirupati 517102, India

Corresponding Author Email: nainaru143@gmail.com

https://doi.org/10.18280/ijht.430318

Received: 26 April 2025
Revised: 16 June 2025
Accepted: 24 June 2025
Available online: 30 June 2025

Keywords:
heat source, Casson fluid, chemical reaction, couple stress

ABSTRACT

This numerical communication presents the effect of heat source (HS) on 3D couple stress Casson fluid (CSCF) via bidirectional Stretching Sheet (SS) with chemical reaction (CR). The Casson liquid model says that the behaviour of non-Newtonian fluid (NNF). The CSCF aid to maintain optimum operating temperature and reduction for device overheating by enhancing heat transfer rate. It plays a vital role in industrial applications like cooling or heating by impingement of jet, turbine, blades, film cooling, mass and heat transfer phenomena. Additionally, studying heat source and chemical reaction in liquid motion contributes to understanding pollutant dispersion from industrial sources and improving combustion efficiency to reduce emissions. In this work, numerical computations are performed to analyze the steady couple stress Casson liquid via SS. The flow problem is based on relevant physical results in a set of PDE which are retarded into ODE's forms. The numerical methodology by help of shooting technique is explore into numerical solutions based on MATLAB programming. The solutions of various physical parameters are explained via graphically in the form of $f'(\eta)$, $\theta(\eta)$ and $\phi(\eta)$ profiles. Moreover, the skin friction coefficient (SFC) via x^*, y^* directions, heat and mass transfer (HMTR). It is observed that the couple stress NNF motion via SS has produce more heat transfer rate (HTR) and mass transfer rate (MTR) when presence of H, Γ_1 (HS, CR effects respectively). Also, the velocity of Casson fluid and HTR is very high for the case of hydromagnetic and HTR generate more in NFs with large numerical values of heat source.

1. INTRODUCTION

The couple stress fluid (CSF) has a motivated work by the upcoming research scientists, because it is utilizing in different physical liquid problems like liquid crystals, colloidal liquids, animal and human blood, lubrication. Moreover, such liquids are used in industrial and engineering like aerodynamic heating, electrostatic precipitation, petroleum products, solidification of liquid crystals, exotic lubricants. The CS fluid ("applications in chemical engineering like fluid crystals, polymer thickened oils, polymeric suspensions and physiological fluid mechanics ext.") was first established by Stokes [1] and is simplest generalization of classical theory of fluids which is polar NNF theories. The theory of couple stress is familiar from theory of elastic shells was presented by Toupin [2]. Srivastava [3] investigated by the CSF model. Mindlin [4] examined the 2D theory of CS model. Srivastava [5] developed under the condition of zero Reynold number in CSF. Yang et al. [6] discussed the classical theory of couple stress. The convection motion of CSF via channel was established [7, 8]. The CSCF motion via bidirectional SS was developed [9-11].

At present modelling of HMT in NN liquid motion via SS have practical and fundamental importance in extensive industrial and production tenders ("bioengineering and polymeric fluids, annealing and thinning of copper wire, nuclear fuel slurries, plasma and mercury,") involved. Huang [12] explained numerically the HMT of NN power law fluid via vertical cone. Oyelakin et al. [13] presented the HMT on the 3D Casson NFs motion by convective conditions. Some of the scientists [14-17] established heat and mass transfer in NN liquids via SS. Mahabaleshwar et al. [18] established Brinkmann model in NN liquid motion on porous shrinking sheet. Recently, the various characteristics NN NFs motion via different channels was found [19-23].

Another most significant work has convective motion regime of temperature, concentration fields an electrically conducting in a SS around a heating or cooling surface. It has more uses in industrial such as cooling of nuclear reactors, thermal insulation, petroleum reservoirs, and geothermal reservoirs ext. The unsteady 3D couple stress liquid via stretching surface with convective condition was discussed by Thammanna et al. [24]. The Casson liquid motion by convective condition via SS was presented [25-29]. The unsteady convective flow of NFs via surface was explained [30-33] numerically. The numerical solutions of convective motion of NFs were established [34, 35]. Marzougui et al. [36] find out that the existence of Hartmann number where the magnetic field dominates via its intrinsic effect.

The primary motivation is to explore realistic flow

conditions commonly found in industrial and biomedical processes, such as extrusion, plastic sheet stretching, and tissue engineering, where both surface stretching and microstructural effects are non-negligible. The bidirectional stretching surface generates a three-dimensional velocity field, adding complexity and practical relevance compared to unidirectional cases.

Novelty arises from the combined consideration of Casson fluid rheology, couple stress theory, internal heat generation, and a homogeneous chemical reaction mechanism within a 3D flow regime an area not widely studied in the current literature. The governing partial differential equations are transformed into a system of ordinary differential equations using similarity transformations. These equations are then solved numerically using an efficient Runge-Kutta-based shooting method.

Limitations:

- The governing equations are highly nonlinear and coupled, making analytical solutions nearly impossible and requiring advanced numerical techniques.
- The Casson model applies only to specific non-Newtonian fluids (e.g., blood, ketchup) and may not be valid for all industrial fluids.
- Bidirectional stretching surfaces are idealized assumptions that may not accurately represent real-world surfaces in practical systems.
- Couple stress and Casson parameters are difficult to measure experimentally, limiting the validation of simulation results.
- Most such studies assume laminar flow; however, in real applications, turbulent effects may be significant and must be considered.
- Nanofluid or particulate effects in multiphase systems are often ignored, limiting accuracy in heterogeneous mixtures.
- Assumes a spatially uniform heat source (HS), which may not reflect varying thermal loads in real-world conditions.

2. MATHEMATICAL FORMULATION

The effect of HS on 3D motion of HMT of an incompressible, convective NN Casson liquid over bidirectional SS was consider at z^*=0 with chemical reaction. In the direction of z^*, we applied MF M_0 and perpendicular to the surface (i.e. x^*y^*-plane) with electrically conducting. The liquid motion occupies the region $z^* > 0$ as it displayed in Figure 1. The stretching velocities $u_1 = U_w^*(x) = a_1 x^*, v_1 = V_w^*(y) = b_1 y^*$ are along in x^* and y^* directions.

The established rheological equation of isotropic and steady Casson liquid motion as [37]:

$$\tau_{ij}^* = \begin{cases} \left(2\mu_0^* + \dfrac{2p_y^*}{\sqrt{2\pi^*}}\right)e_{ij}, & \pi^* \geq \pi_1^* \\ \left(2\mu_0^* + \dfrac{2p_y^*}{\sqrt{2\pi_1^*}}\right)e_{ij}, & \pi^* < \pi_1^* \end{cases} \tag{1}$$

where, $\pi^* = e_{ij}e_{ij}$ and $p_y^* = \mu_0^*\sqrt{2\pi^*}/\beta^*$ with the consideration. The established governing equations continuity, heat and concentration equations for the BL motion as taken following forms [24]:

$$\frac{\partial u_1}{\partial x^*} + \frac{\partial v_1}{\partial y^*} + \frac{\partial w_1}{\partial z^*} = 0 \tag{2}$$

$$\left.\begin{aligned} u_1\frac{\partial u_1}{\partial x^*} + v_1\frac{\partial u_1}{\partial y^*} + w_1\frac{\partial u_1}{\partial z^*} &= \upsilon^*\left(1+\frac{1}{\beta^*}\right)\frac{\partial^2 u_1}{\partial\left(z^*\right)^2} \\ &\quad -\left(\upsilon^*\right)'\frac{\partial^4 u_1}{\partial\left(z^*\right)^4} - \frac{\sigma^* M_0^2}{\rho^*}u_1 \end{aligned}\right\} \tag{3}$$

$$\left.\begin{aligned} u_1\frac{\partial v_1}{\partial x^*} + v_1\frac{\partial v_1}{\partial y^*} + w_1\frac{\partial v_1}{\partial z^*} &= \upsilon^*\left(1+\frac{1}{\beta^*}\right)\frac{\partial^2 v_1}{\partial\left(z^*\right)^2} \\ &\quad -\left(\upsilon^*\right)'\frac{\partial^4 v_1}{\partial\left(z^*\right)^4} - \frac{\sigma^* M_0^2}{\rho^*}v_1 \end{aligned}\right\} \tag{4}$$

$$u_1\frac{\partial T^*}{\partial x^*} + v_1\frac{\partial T^*}{\partial y^*} + w_1\frac{\partial T^*}{\partial z^*} = \alpha_m^*\frac{\partial^2 T^*}{\partial\left(z^*\right)^2} - \frac{Q_0^*}{(\rho^* C)_f}(\mathrm{T}^* - \mathrm{T}_\infty^*) \tag{5}$$

$$u_1\frac{\partial C^*}{\partial x^*} + v_1\frac{\partial C^*}{\partial y^*} + w_1\frac{\partial C^*}{\partial z^*} = D^*\frac{\partial^2 C^*}{\partial\left(z^*\right)^2} - K_1^*(\mathrm{C}^* - \mathrm{C}_\infty^*) \tag{6}$$

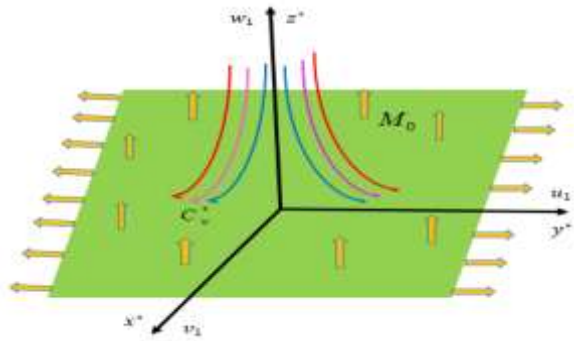

Figure 1. Physical modeling of the problem

The relevant BC of the present model as:

$$\left.\begin{aligned} &u_1 = a_1 x^*,\ \mathrm{v} = by,\ \mathrm{w}_1 = 0, \\ &-k^*\frac{\partial T^*}{\partial z^*} = h_1^*(\mathrm{T}_f^* - \mathrm{T}^*),\ -D^*\left(\frac{\partial C^*}{\partial z^*}\right) = h_2^*\left(C_f^* - C^*\right),\ \text{at}\ \mathrm{z}^* = 0 \\ &u_1 \to 0,\ v_1 \to 0,\ u_1' \to 0, \\ &v_1' \to 0,\ T^* \to T_\infty^*,\ C^* \to C_\infty^*,\quad as\quad z^* \to \infty \end{aligned}\right\} \tag{7}$$

The similarity transformations as below:

$$\left.\begin{aligned} &\eta_1 = \sqrt{\frac{a_1}{\upsilon_f^*}}z^*,\quad u_1 = a_1 x^* f'(\eta_1),\quad v_1 = a_1 y^* g'(\eta_1), \\ &\mathrm{w}^* = -\sqrt{a_1\upsilon^*}\,(f(\eta_1) + g(\eta_1)) \\ &\theta(\eta_1) = \frac{T^* - T_\infty^*}{T_w^* - T_\infty^*},\quad \phi(\eta_1) = \frac{C^* - C_\infty^*}{C_w^* - C_\infty^*} \end{aligned}\right\} \tag{8}$$

Using above Eq. (8), we are converting Eqs. (3)-(6) into

below format:

$$K_1 f^{v} + \mathrm{M}_1 f' - f'''(1+\frac{1}{\beta^*}) - f''(f+\mathrm{g}) + (f')^2 = 0 \quad (9)$$

$$K_1 g^{v} + \mathrm{M}_1 \mathrm{g}' - g'''(1+\frac{1}{\beta^*}) - g''(f+\mathrm{g}) + (g')^2 = 0 \quad (10)$$

$$\theta'' + \mathrm{Pr}(f+\mathrm{g})\theta' - H_1 \mathrm{Pr}\,\theta = 0 \quad (11)$$

$$\phi'' - \mathrm{Pr}\,Le\left((f+\mathrm{g})\phi' + \gamma^*\phi\right) = 0 \quad (12)$$

Corresponding B. Cs as below:

$$\left.\begin{array}{l} \eta_1 = 0 \;\; as \;\; f = 0, \quad g = 0, \quad f' = 1, \\ g' = \lambda^*, \quad \theta' = -\gamma_1(1-\theta), \;\; \phi' = -\gamma_2(1-\phi) \end{array}\right\} \left.\begin{array}{l} \\ \\ \\ \end{array}\right\} \quad (13)$$
$$\left.\begin{array}{l} \eta_1 \to \infty \;\; at \;\; f' \to 0, \;\; g' \to 0, \\ f'' \to 0, \;\; g'' \to 0, \;\; \theta \to 0, \;\; \phi \to 0 \end{array}\right\}$$

Moreover, the skin-friction coefficient and Nusselt number are below:

$$\left.\begin{array}{l} \mathrm{Re}_x^{1/2} C_{fx} = (1+\beta^*/\beta^*) f''(0) - \mathrm{K}_1 f^{v}(0), \\ \mathrm{Re}_x^{1/2} C_{fy} = (1+\beta^*/\beta^*) \mathrm{g}''(0) - \mathrm{K}_1 \mathrm{g}^{v}(0) \\ \mathrm{Re}_x^{-1/2} Nu_x = -\theta'(0), \;\; \mathrm{ShRe}_x^{-1/2} = -\phi'(0) \end{array}\right\} \quad (14)$$

3. RESULTS AND DISCUSSION

The CSCF characteristics of λ^* on velocity motion along x^*, y^*-axis $(f'(\eta_1), g'(\eta_1))$ and $\theta(\eta_1)$ as illustrated respectively in Figure 2 and Figure 3. It is perceived that, the $(f'(\eta_1), g'(\eta_1))$ (axial, transverse velocities resp.) smoothly convergence (point at surface area is λ^*=0.8 (not exact value)) monotonically increases along with x^*, y^* axis and associated BL thickness of couple stress NN liquid motion is thinner with ascending numerical values of λ^*. Physically, when stretching ratio increase in NN CS liquid from zero then the lateral surface begins to move in the x^*, y^* axis rises and $\theta(\eta_1)$ monotonically down for $(K_1 = \beta^* \to \infty)$ and $(K_1 = \beta^* = 0.5)$. For these cases, the results are mentioned that $\theta(\eta_1)$ is more effected in pure fluid case $(K_1 = \beta^* \to \infty)$ than NN CS fluid $(K_1 = \beta^* = 0.5)$.

Figure 4 and Figure 5 predict the effect of K_1 on $(f'(\eta_1), g'(\eta_1))$ and $\theta(\eta_1)$. It is analysed that, the speed of NN liquid is enhances along with x^* and y^* directions whereas reverse trend behaviour shows $\theta(\eta_1)$ for distinct enlarge values of K_1. Physically, the CS parameter is inversely proportional to Kinematic viscosity because it reflects the relative influence of microstructural (rotational or size-dependent) effects in a fluid compared to standard viscous (shear) diffusion.

The most significant characteristic M_1 on $(f'(\eta_1), g'(\eta_1))$ respectively presented in Figures 6-9. It is dictated that, the velocity in y^*- axis $g'(\eta_1)$ is high convergence deference than the x^*-axis velocity $f'(\eta_1)$ and also $Re_x^{1/2} C_{fx}$, $Re_x^{1/2} C_{fy}$ (skin friction coefficients) rises in fluid motion along in x^*, y^*-axis while opposite behaviours $\theta(\eta_1)$ profile with growth numerical values of M_1. Physically, the Lorentz force applied to liquid flow direction which is stronger to high magnetic field in NN couple stress liquid and then, the energy is transformed into heat because of friction forces.

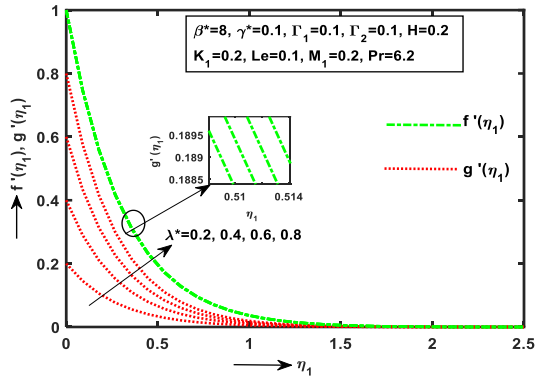

Figure 2. Effect of λ^* on $f'(\eta_1)$, g'(η_1)

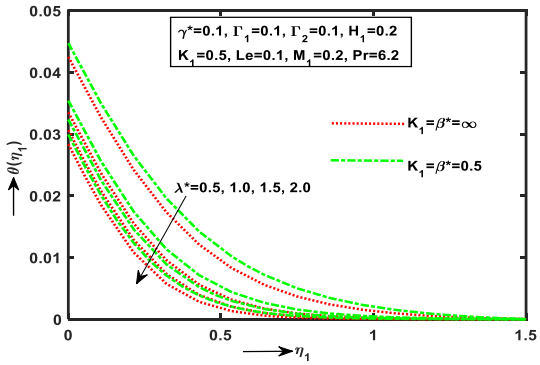

Figure 3. Effect of λ^* on $\theta(\eta_1)$

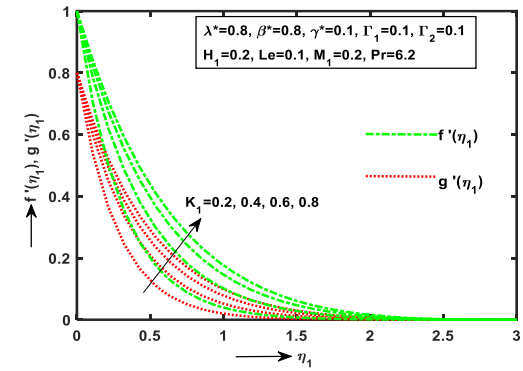

Figure 4. Effect of K_1 on $f'(\eta_1)$, g'(η_1)

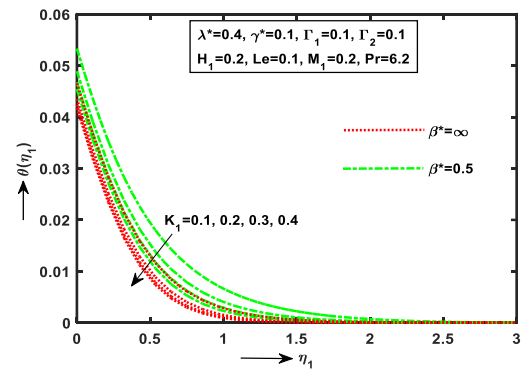

Figure 5. Effect of K_1 on $\theta(\eta_1)$

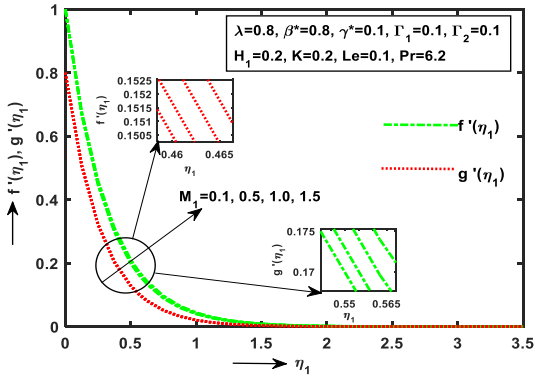

Figure 6. Effect of M_1 on $f'(\eta_1)$, $g'(\eta_1)$

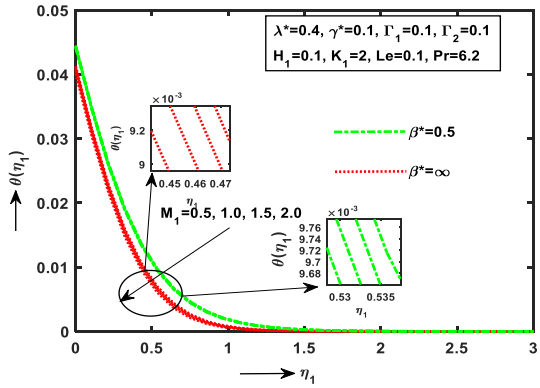

Figure 7. Effect of M_1 on $\theta(\eta_1)$

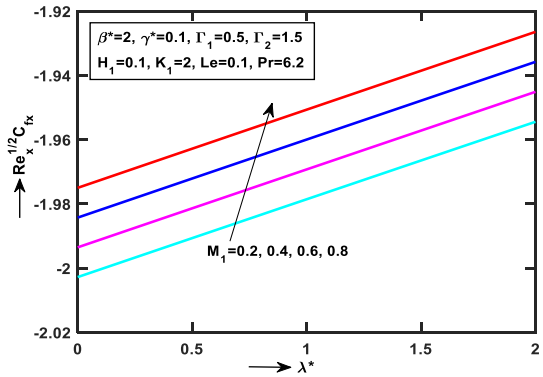

Figure 8. Effect of M_1 on $\mathrm{Re}_x^{1/2} C_{fx}$

Figure 10 and Figure 11 predict the significant parameter β^* on velocity profiles $(f'(\eta_1), g'(\eta_1))$ and corresponding high BL thickness convergence to η_1=0.8 with enlarge numerical values of β^*. Figure 11 presents that the $Re_x^{-1/2} N u_x$ is enlarges in various magnetic field conditions (like M_1=0.5 (hydromagnetic), M_1=0.0 (hydrodynamic) and M_1=-0.5 (terminating field lines)). In CSCF motion involved multiple charges, the magnetic field generate more heat transfer $\left(Re_x^{-1/2} N u_x\right)$ in M_1=0.5 positive charges, the field is negative M_1=-0.5 than the heat transfer rate $\left(Re_x^{-1/2} N u_x\right)$ is terminating and field should be zero there is no heat transfer $\left(Re_x^{-1/2} N u_x\right)$ on stretching surface. Physically, the CF parameter is proportional to dynamic viscosity, it is produced resistance force in the flow is very high and higher values of β^*. Further, this fluid parameter depends on yield stress of fluid and drag the thinner BL thickness of the fluid flow towards a stretching surface.

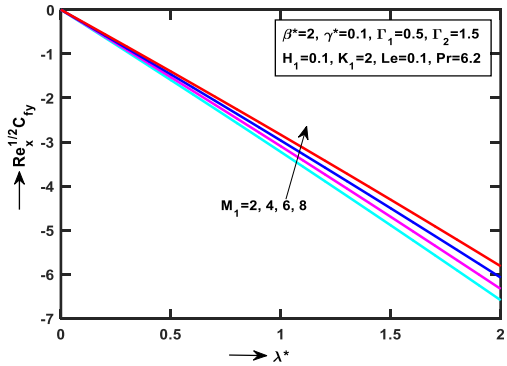

Figure 9. Effect of M_1 on $\mathrm{Re}_x^{1/2} C_{fy}$

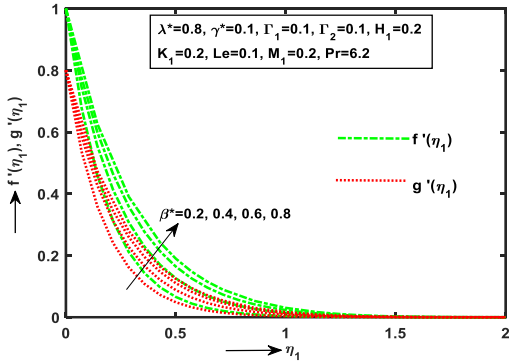

Figure 10. Effect of β on $f'(\eta)$, $g'(\eta)$

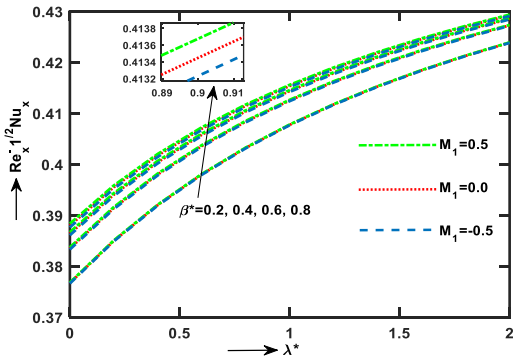

Figure 11. Effect of β on $Nu_x \mathrm{Re}_x^{-1/2}$

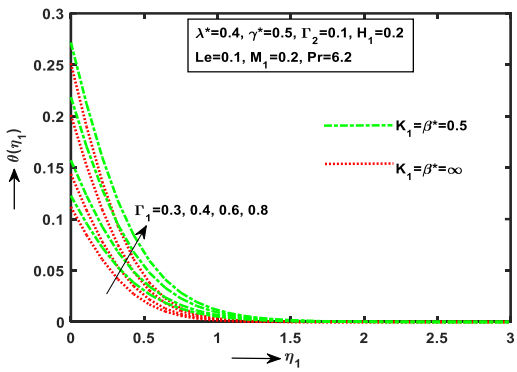

Figure 12. Effect of Γ_1 on $\theta(\eta_1)$

Variation of $\theta(\eta_1)$ for $(K_1 = \beta^* = 0.5)$ and $(K_1 = \beta^* \to \infty)$, $Re_x^{-1/2} N u_x$ for the cases of $(\beta^* = 0.5)$ (CSCF) and $(\beta^* \to \infty)$ (couple stress fluid) enhances with distinct ascending numerical values of Γ_1 (temperature Biot number) as depicted in Figure 12 and Figure 13, respectively. It is dictates that the stronger intensity of convective heat, the high thermal BL convergence in Newtonian liquid $(K_1 = \beta^* \to \infty)$ while comparing NN fluid $(K_1 = \beta^* = 0.5)$ and moreover, $Re_x^{-1/2} N u_x$ is more significant in CS fluid $(\beta^* \to \infty)$ is better than CSCF $(\beta^* = 0.5)$ with ascending values of Γ_1. Physical representation as a measure of the ratio of convective heat transfer at the surface to conductive heat transfer within the fluid. It characterizes how effectively heat is exchanged between the fluid and the stretching surface.

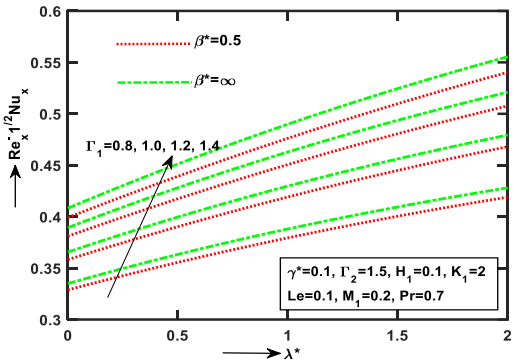

Figure 13. Effect of Γ_1 on $Nu_x\mathrm{Re}_x^{-1/2}$

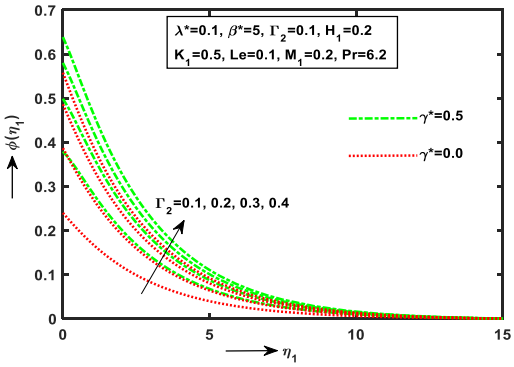

Figure 14. Effect of Γ_2 on $\phi(\eta_1)$

Figure 14 illustrates that the profile $\phi(\eta_1)$ enlarges with numerical values of Γ_2 (concentration Biot number) for the presence $(\gamma^* = 0.5)$ and absence $(\gamma^* = 0.0)$ of CR. It is declined that, the weaker intensity of convective concentration in liquid motion, the ascending $\phi(\eta_1)$ monotonically convergent to surface of the point $(\eta_1 = 9.5)$. The NN couple stress fluid generate heat is more when absence $(\gamma^* = 0.0)$ of chemical reaction while comparing presence $(\gamma^* = 0.5)$ of chemical reaction with ascending values of Γ_2. Physical reason represents the ratio of MT at the boundary (surface) to mass diffusion within the fluid. It provides a physical measure of how effectively a solute (or chemical species) is transported across the fluid–surface interface compared to its internal diffusion.

The variation of H_1 on $\mathrm{Re}_x^{-1/2}Nu_x$ for Casson couple stress fluid $(K^* = \beta^* = 0.5)$ and pure fluid $(K^* = \beta^* \to \infty)$ as expressed in Figure 15. The heat transfer $\mathrm{Re}_x^{-1/2}Nu_x$ is high with enlarge values of H_1. It is clear view of $\mathrm{Re}_x^{-1/2}Nu_x$ is more effected in pure fluid $(K^* = \beta^* \to \infty)$ while comparison of CSCF (NN CS fluid) $(K^* = \beta^* = 0.5)$. Physically, the HS is inversely proportional to fluid density. Due to this the isothermal temperature and heat transfer rate high in CS liquid motion towards from stretching surface with enhances values of H_1.

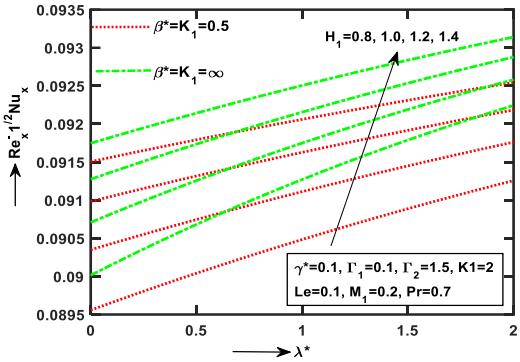

Figure 15. Effect of H_1 on $Nu_x\mathrm{Re}_x^{-1/2}$

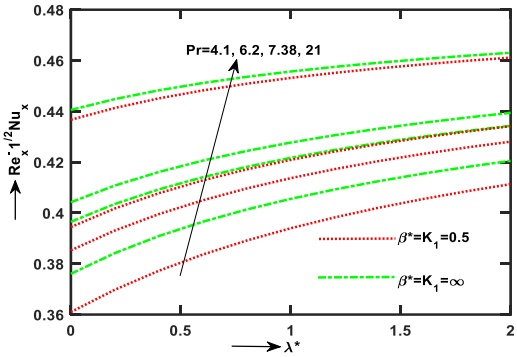

Figure 16. Effect of Pr on $Nu_x\mathrm{Re}_x^{-1/2}$

The most significant physical number is Pr (Prandtl number) on $\left(Re_x^{-1/2} N u_x\right)$ with various Thermophysical fluid values of Pr (such as CO_2=4.1, H_2O=6.2, CH_3OH=7.38, $C_{12}H_{26}$=21) as predict respectively in Figure 16. It is discussed on $(\mathrm{Re}_x^{-1/2}Nu_x)$ in two cases one is pure fluid $(K_1 = \beta^* \to \infty)$ and second one is NN CS liquid case $(K_1 = \beta^* = 0.5)$. Which is clear that, the couple stress non-Newtonian $(K_1 = \beta^* = 0.5)$ fluid has produced more heat transfer when compared to the pure fluid $(K_1 = \beta^* \to \infty)$. Physically, the Prandtl number is ratio between the viscous diffusion rate and thermal diffusion rate. The thermal diffusion rate is more in CSCF motion then pure fluid, so that the HTR is produce high in surface.

Figure 17 illustrates that the profile $\phi(\eta_1)$ enlarges with distinct higher numerical values of y^* (CR parameter) while reverse behaviours displays $\mathrm{ShRe}_x^{-1/2}$ (MTR) for presence convective Biot numbers $\Gamma_1, \Gamma_2 = 0.5$ and absence of Biot numbers $\Gamma_1, \Gamma_2 = 0.0$ as seen in Figure 18. It is demonstrated that, the $\mathrm{ShRe}_x^{-1/2}$ is produce more in presence of $\Gamma_1, \Gamma_2 = 0.5$ while comparing absence of Biot number $(\Gamma_1, \Gamma_2 = 0.0)$. Physical represents the rate at which a chemical species is generated or consumed within the fluid flow due to a chemical reaction. It directly influences the concentration distribution and indirectly affects mass transfer and possibly thermal or rheological properties, depending on the nature of the reaction.

Table 1. Comparison of Skin friction coefficient $\left(1+\frac{1}{\beta^*}\right)f''(0)$ in the absence of $(K_1=0)$

M_1	β^*	Present Study	Sarah et al. [38]	Nadeem et al. [39]	Gupta and Sharma [40]	Ahmad and Nazar [41]
0.0	∞	1.000000000	1.0000	1.0004	1.0003	1.004
	1.0	1.414214	1.4142	1.414	1.4142	-
	2.5	1.183215	-	-	-	-
	3.5	1.133893	-	-	-	-
	5.0	1.095445	1.0954	1.095	1.0954	-
10	∞	3.316624	3.3166	3.316	3.3165	3.316
	1.0	4.690415	4.6904	4.690	4.6904	-
	2.5	3.924283	-	-	-	-
	3.5	3.760699	-	-	-	-
	5.0	3.633180	3.6331	3.633	3.6331	-
100	∞	10.04987	10.049	10.04	10.049864	10.04
	1.0	14.21670	14.212	14.21	14.212	-
	2.5	11.89117	-	-	-	-
	3.5	11.39548	-	-	-	-
	5.0	11.00908	11.009	11.00	11.009	-

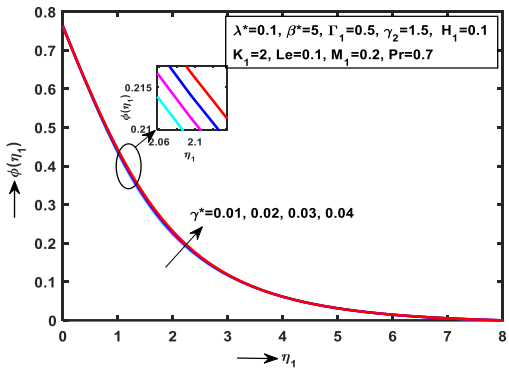

Figure 17. Effect of y^* on $\phi(\eta_1)$

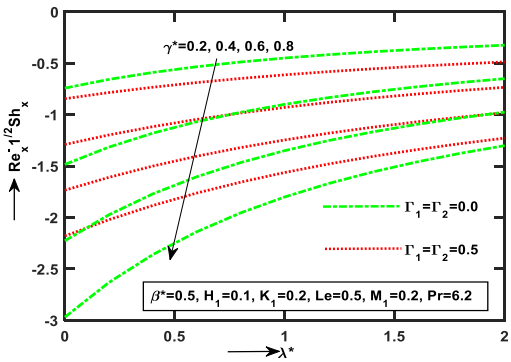

Figure 18. Effect of y^* on $ShRe_x^{-1/2}$

Characterise of *Le* (Lewis number) with absence and presence of Casson fluid ($\beta^* = 0.5$) (like CSCF) and absence of Casson fluid ($\beta^* \to \infty$) (like CSCF) on $ShRe_x^{-1/2}$ displays in Figure 19. In view of this the $ShRe_x^{-1/2}$ profile enlarges with distinct ascending values of *Le*. It is finally concluded that, the couple stress fluid ($\beta^* = 0.5$) is produce high MTR while comparing Casson couple stress fluid ($\beta^* \to \infty$). Physically, it describes the relative efficiency of heat diffusion compared to mass (species) diffusion in the fluid.

The present effort computes numerical results via R-K-F 4th order along with shooting technique is matched up to four decimal places and also find extra numerical results. the present results compared to related articles of Sarah et al. [38], Nadeem et al. [39], Gupta and Sharma [40] and Ahmad and Nazar [41] for some specific cases (like K_1=0 and λ=1.0) and getting good agreement results (Table 1 and Table 2) respectively.

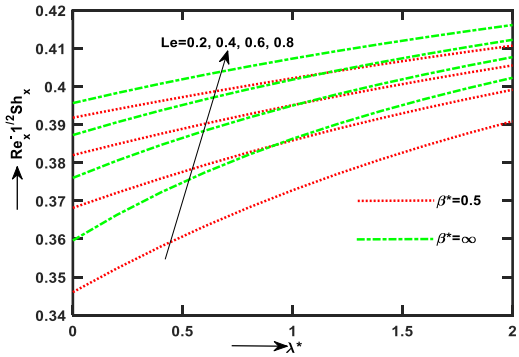

Figure 19. Effect of *Le* on $ShRe_x^{-1/2}$

Table 2. Comparison of skin friction coefficient in the absence of (K_1=0) and λ^*=1.0

M_1	β^*	Present Study	Nadeem et al. [39]
0.0	∞	1.173719025	--
	1.0	1.659891956	1.6599
	2.5	1.388765332	--
	3.5	1.330874747	--
	5.0	1.285747074	1.2857
10	∞	3.367222224	3.3667
	1.0	4.761964421	4.7620
	2.5	3.984161191	--
	3.5	3.818079080	--
	5.0	3.688613149	3.6886
100	∞	10.06646642	10.066
	1.0	14.23613181	14.2361
	2.5	11.91079007	---
	3.5	11.41428580	---
	5.0	11.55856650	11.0272

Table 3 explored the numerical results of heat transfer rates with respect to variation of various physical parameters. The $Re_x^{-1/2}Nu_x$ amplify for ascending values of K_1, Pr, M_1, H_1, Γ_1, and β^* respectively.

The mass transfer rates of different parameters demonstrated in Table 4. The (MTR) $Re_x^{-1/2}Sh$ decline with enlarge numerical values of K_1, M_1, γ^* and β^* while opposite trend with enhance values of Pr, *Le* when presence $\Gamma_1 = 0.5 =$

Γ_2 and absence $\Gamma_1 = 0 = \Gamma_2$ of temperature and concentration Biot number, respectively.

Table 3. Numerical values of $Re_x^{-1/2}Nu_x$ with different parameters of K_1, Le, Pr, R_d, M_1, N_t, N_b, θ_w, H_1, Γ_1, Γ_2, γ^*, Ec_x, and Ec_y for λ^*=0

K_1	Pr	M_1	H_1	Γ_1	β^*	$Re_x^{-1/2}Nu_x$
0.5						0.2924
1						0.296
1.5						0.2979
2						0.2992
	0.5					0.0834
	1					0.0871
	1.5					0.0893
	2					0.0907
		0.5				0.0851
		1				0.0856
		1.5				0.0856
		2				0.0856
			0.5			0.0885
			1			0.0906
			1.5			0.0919
			2			0.0927
				0.5		0.2673
				1		0.3648
				1.5		0.4153
				2		0.4462
					0.5	0.0848
					1	0.085
					1.5	0.0861
					2	0.0861

Table 4. Numerical values of $Re_x^{-1/2}$Sh with different parameters of K_1, Pr, R_d, M_1, θ_w, H_1, γ^*, Ec_x, and Ec_y for λ^*=0

K_1	Pr	Le	M_1	γ^*	β^*	$Re_x^{-1/2}$Sh	
						$\Gamma_1 = 0 = \Gamma_2$	$\Gamma_1 = 0.5 = \Gamma_2$
0.5						0.0397	-0.8907
1						0.0387	-0.5931
1.5						0.038	-0.5946
2						0.0374	-0.5956
	0.5					0.0264	-0.6037
	1					0.0542	-0.6071
	1.5					0.0833	-0.6103
	2					0.1139	-0.6132
		0.5				0.1074	-0.5408
		1				0.2582	-0.4673
		1.5				0.4708	-0.3787
		2				0.7719	-0.2775
			0.5			0.0374	-0.6052
			1			0.0374	-0.6053
			1.5			0.0373	-0.6054
			2			0.0373	-0.6055
				0.5		0.09355	-0.5744
				1		0.1871	-0.5392
				1.5		0.2803	-0.504
				2		0.3742	-0.4687
					0.5	0.03479	-0.5976
					1	0.0342	-0.5984
					1.5	0.03399	-0.5987
					2	0.03388	-0.5989

4. CONCLUSION

This work we have deals with the SH effect on 3D convective flow of non-Newtonian couple stress fluid over bidirectional stretching surface with chemical reaction. The significant results noticed a follows:

- Under hydromagnetic conditions, the Lorentz force enhances the flow dynamics of the Casson fluid, resulting in elevated velocity and an increased rate of heat transfer.
- An increase in the Temperature Biot number signifies stronger surface convection, which enhances heat transfer into the Casson fluid and raises its internal temperature.
- In a pure fluid, a high heat source parameter indicates intense internal heat generation, which boosts the thermal energy within the fluid and consequently enhances the heat transfer rate.
- The chemical reaction parameter increases the concentration boundary layer thickness, but it simultaneously reduces the mass transfer rate, with this opposing behavior observed both in the absence and presence of temperature and concentration Biot numbers due to altered diffusion and reactive resistance near the surface.

REFERENCES

[1] Stokes, V.K. (1984). Couple stresses in fluids. In Theories of Fluid with Microstructure. Springer, Berlin, Heidelberg, pp. 34-80. https://doi.org/10.1007/978-3-642-82351-0_4

[2] Toupin, R.A. (1964). Theories of elasticity with couple stress. Archive for Rational Mechanics and Analysis, 17: 85-112. https://doi.org/10.1007/BF00253050

[3] Srivastava, L.M. (1985). Flow of couple stress fluid through stenotic blood vessels. Journal of Biomechanics, 18(7): 479-485. https://doi.org/10.1016/0021-9290(85)90662-1

[4] Mindlin, R.D. (1963). Influence of couple stresses on stress concentration. Experimental Mechanics, 3: 1-7. https://doi.org/10.1007/BF02327219

[5] Srivastava, L.M. (1985). peristaltic transport of a couple stress fluid. Rheologica Acta, 25: 638-641. https://doi.org/10.1007/BF01358172

[6] Yang, F., Chong, A.C.M., Lam, D.C.C., Tong, P. (2002). Couple stress-based strain gradient theory for elasticity. International Journal of Solids and Structures, 39(10): 2731-2743. https://doi.org/10.1016/S0020-7683(02)00152-X

[7] Eegunjobi, A.S., Makinde, O.D. (2017). Irreversibility analysis of hydromagnetic flow of couple stress fluid with radiation heat in a channel filled with a porous medium. Results in Physics, 7: 459-459. https://doi.org/10.1016/j.rinp.2017.01.002

[8] Adesanya, S.O., Makhalemele, C.R., Rundora, L. (2017). Natural convection flow of heat generating hydromagnetic couple stress fluid with time periodic boundary conditions. Alexandria Engineering Journal, 57(3): 1977-1989. https://doi.org/10.1016/j.aej.2017.04.006

[9] Hayat, T., Muhammad, T., Alsaedi, A. (2017). On three-dimensional flow of couple stress fluid with Cattaneo-Christov heat flux. Chinese Journal of Physics, 55(3): 930-938. https://doi.org/10.1016/j.cjph.2017.03.003

[10] Mahabaleshwar, U.S., Sarris, I.E., Hill, A.A., Lorenzini, G., Pop, I. (2017). An MHD couple stress fluid due to a perforated sheet undergoing linear stretching with heat transfer. International Journal of Heat and Mass Transfer,

105: 157-167. https://doi.org/10.1016/j.ijheatmasstransfer.2016.09.040
[11] Ali, N., Khan, S.U., Sajid, M., Abbas, Z. (2016). MHD flow and heat transfer of couple stress fluid over an oscillatory stretching sheet with heat source/sink in porous medium. Alexandria Engineering Journal, 55(2): 915-924. https://doi.org/10.1016/j.aej.2016.02.018
[12] Huang, C.J. (2018). Effects of internal heat generation and Soret/Dufour on natural convection of non-Newtonian fluids over a vertical permeable cone in a porous medium. Journal of King Saud University – Science, 30(1): 106-111. https://doi.org/10.1016/j.jksus.2016.09.009
[13] Oyelakin, I.S., Mondal, S., Sibanda, P. (2017). Unsteady MHD three-dimensional Casson nanofluid flow over a porous linear stretching sheet with slip condition. Frontiers in Heat and Mass Transfer, 8(37): 1-9. https://doi.org/10.5098/hmt.8.37
[14] Rahimi, J., Ganji, D.D., Khaki, M., Hosseinzadeh, K.H. (2016). Solution of the boundary layer flow of an Eyring-Powell non-Newtonian fluid over a linear stretching sheet by collocation method. Alexandria Engineering Journal, 56(4): 621-627. https://doi.org/10.1016/j.aej.2016.11.006
[15] Uddin, M.J., Rashidi, M.M., Alsulami, HH., Abbasbandy, S., Freidoonimeh, N. (2016). Two parameters lie group analysis and numerical solution of unsteady free convective flow of non-Newtonian fluid. Alexandria Engineering Journal, 55(3): 2299-2308. https://doi.org/10.1016/j.aej.2016.05.009
[16] Rashidi, M.M., Bagheri, S., Momoniat, E., Freidoonimehr, N. (2017). Entropy analysis of convective MHD flow of third grade non-Newtonian fluid over a stretching sheet. Ain Shams Engineering Journal, 8(1): 77-85. https://doi.org/10.1016/j.asej.2015.08.012
[17] Raju, C.S.K., Sandeep, N., Malvandi, A. (2016). Free convective heat and mass transfer of MHD non-Newtonian nanofluids over a cone in the presence of non-uniform heat source/sink. Journal of Molecular Liquids, 221: 108-115. https://doi.org/10.1016/j.molliq.2016.05.078
[18] Mahabaleshwar, U.S., Vishalakshi, A.B., Azese, M.N. (2022). The role of Brinkmann ratio on non-Newtonian fluid flow due to a porous shrinking/stretching sheet with heat transfer. European Journal of Mechanics - B/Fluids, 92: 153-165. https://doi.org/10.1016/j.euromechflu.2021.12.003
[19] Ananth Kumar, K., Sugunamma, V., Sandeep, N. (2019). Numerical examination of MHD nonlinear radiative slip motion of non-Newtonian fluid across a stretching sheet in the presence of a porous medium. Heat Transfer, 50(12): 1163-1181. https://doi.org/10.1615/HeatTransRes.2018026700
[20] Mishra, S.R., Shamshuddin, MD., Anwar Beg, O., Kadir, A. (2020). Adomain computation of radiative-convective bi-directional stretching flow of a magnetic non-Newtonian fluid in porous media with homogeneous-heterogeneous reactions. International Journal of Modern Physics, 34(18): 2050165. https://doi.org/10.1142/S0217979220501659
[21] Anantha Kumar, K., Ramoorthy Reddy, B., Sandeep, N., Sugunamma, V. (2020). Effect of joule heating on MHD non-Newtonian fluid flow past an exponentially stretching curved surface. Heat Transfer, 49(6): 3575-3592. https://doi.org/10.1002/htj.21789
[22] Ramesh, B.K., Misbah, N.E. (2020). Hydrodynamic flow of non- Newtonian power-law fluid past a moving wedge or a stretching sheet: A unified computational approach. Scientific Reports, 10: 9445. https://doi.org/10.1038/s41598-020-66106-6
[23] Ali, R., Asjad, M.I., Aldalbahi, A., Gorji, M.R., Rahaman, M. (2021). Convective flow of a maxwell hybrid nanofluid due to pressure gradient in a channel. Journal of Thermal Analysis and Calorimetry, 143: 1319-1329. https://doi.org/10.1007/s10973-020-10304-x
[24] Thammanna, G.T., Ganesh Kumar, K., Gireesha, B.J., Ramesh, G.K., Prasannakumara, B.C. (2017). Three dimensional MHD flow of couple stress Casson fluid past an unsteady stretching surface with chemical reaction. Results in Physics, 7: 4104-4110. https://doi.org/10.1016/j.rinp.2017.10.016
[25] Gireesha, B.J., Archana, M., Prasannakumara B.C., Reddy Gorla, R.S., Makinde, O.D. (2017). MHD three-dimensional double diffusive flow of Casson nanofluid with buoyancy forces and nonlinear thermal radiation over a stretching surface. International Journal of Numerical Methods for Heat & Fluid Flow, 27(12): 2858-2878. https://doi.org/10.1108/HFF-01-2017-0022
[26] Awais, M., Saleem, S., Hayat, T., Irum, S. (2016). Hydromagnetic couple-stress nanofluid flow over a moving convective wall: OHAM analysis. Acta Astronautica, 129: 271-276. https://doi.org/10.1016/j.actaastro.2016.09.020
[27] Othman, N.A., Yacob, N.A., Bachok, N., Ishak, A., Pop, I. (2017). Mixed convection boundary-layer stagnation point flow past a vertical stretching/shrinking surface in a nanofluid. Applied Thermal Engineering, 115: 1412-1417. https://doi.org/10.1016/j.applthermaleng.2016.10.159
[28] Mahanthesh, B., Gireesha, B.J., Subba Reddy Gorla, R. (2017). Unsteady three-dimensional MHD flow of a nano Eyring Powell fluid past a convectively heated stretching sheet in the presence of thermal radiation, viscous dissipation and Joule heating. Journal of the Association of Arab Universities for Basic and Applied Sciences, 23: 75-84. https://doi.org/10.1016/j.jaubas.2016.05.004
[29] Hayat, T., Hussain, S., Muhammad, T., Alsaedi, A., Ayub, M. (2017). Radiative flow of Powell-Eyring nanofluid with convective boundary conditions. Chinese Journal of Physics, 55(4): 1523-1538. https://doi.org/10.1016/j.cjph.2017.05.009
[30] Maqbool, K., Mann, A.B., Tiwana, M.H. (2017). Unsteady MHD convective flow of a Jeffery fluid embedded in a porous medium with ramped wall velocity and temperature. Alexandria Engineering Journal, 57(2): 1071-1078. https://doi.org/10.1016/j.aej.2017.02.012
[31] Alam, M.S., Asiyakhatun, M., Rahman, M.M., Vajravelu, K. (2016). Effects of variable fluid properties and thermophoresis on unsteady forced convective boundary layer flow along a permeable stretching/shrinking wedge with variable Prandtl and Schmidt numbers. International Journal of Mechanical Sciences, 105: 191-205. https://doi.org/10.1016/j.ijmecsci.2015.11.018
[32] Chakraborty, T., Das, K., Kundu, P.K. (2016). Framing the impact of external magnetic field on bioconvection of a nanofluid flow containing gyrotactic microorganisms with convective boundary conditions. Alexandria

Engineering Journal, 57(1): 61-71. https://doi.org/10.1016/j.aej.2016.11.011
[33] Mandal, D.P.G., Vajravalu, K. (2016). Soret and Dufour effects on MHD convective–radiative heat and mass transfer of nanofluid over a vertical non-linear stretching/shrinking sheet. Applied Mathematics and Computation, 287-288: 184-200. https://doi.org/10.1016/j.amc.2016.04.037
[34] Ullah, N., Nadeem S., Khan, A.U. (2021). Finite element simulations for natural convective flow of nanofluid in a rectangular cavity having corrugated heated rods. Journal of Thermal Analysis and Calorimetry, 143: 4169-4181. https://doi.org/10.1007/s10973-020-09378-4
[35] Mokaddes Ali, M., Alim, M.A., Ahmed, S.S. (2019). Oriented magnetic field effect on mixed convective flow of nanofluid in a grooved channel with internal rotating cylindrical heat source. International Journal of Mechanical Sciences, 151: 385-409. https://doi.org/10.1016/j.ijmecsci.2018.11.027
[36] Marzougui, S., Oudina, F.M., Assia, A., Magherbi, M., Shah, Z., Ramesh, K. (2021). Entropy generation on magneto-convective flow of copper-water nanofluid in a cavity with chamfers. Journal of Thermal Analysis and Calorimetry, 143: 2203-2214. https://doi.org/10.1007/s10973-020-09662-3
[37] Nakamura, M., Sawada, T. (1988). Numerical study on the flow of a non-Newtonian fluid through an axisymmetric stenosis. Journal of Biomechanical Engineering, 110(2): 137-143. https://doi.org/10.1115/1.3108418
[38] Sarah, I., Mondal, S., Sibanda, P. (2015). Unsteady Casson nanofluid flow over a stretching sheet with thermal radiation, convective and slip boundary conditions. Alexandria Engineering Journal, 55(2): 1025-1035. https://doi.org/10.1016/j.aej.2016.03.003
[39] Nadeem, S., Haq, R.U., Akbar, N.S. (2014). MHD three-dimensional boundary layer flow of Casson nanofluid past a linearly stretching sheet with convective boundary condition. IEEE Transactions on Nanotechnology, 13(1): 109-115. https://doi.org/10.1109/TNANO.2013.2293735
[40] Gupta, S., Sharma, K. (2017). Numerical simulation for magnetohydrodynamic three- dimensional flow of Casson nanofluid with convective boundary conditions and thermal radiation. Engineering Computations, 34(8): 2698-2722. https://doi.org/10.1108/EC-02-2017-0064
[41] Ahmad, K., Nazar, R. (2011). Magnetohydrodynamic three-dimensional flow and heat transfer over a stretching surface in a viscoelastic fluid is discussed. Journal of Science and Technology, 3(1): 1-14.

NOMENCLATURE

a_1	channel length
b_1	thermal slip parameter
u_1, v_1, w_1	velocity components along x^*, y^*, z^*
C^*	nanoparticle volume fraction
C_∞^*	uniform ambient concentration (kgm^{-3})
C_w^*	variable concentration (kgm^{-3})
D_T	thermophoresis diffusion $(m^2.s^{-1})$
D_B	Brownian diffusion
f	dimensionless stream function
f'	dimensionless velocity
K_1	couple stress parameter= $\frac{a_1(\upsilon^*)\prime}{(\upsilon^*)^2}$
Le	Lewis number= $\frac{\alpha_m^*}{D_B}$
M_1	magnetic field parameter= $\frac{\sigma^* M_0^2}{a_1 \rho_f}$
Pr	Prandtl number= $\left(\frac{\upsilon^*}{\alpha_m^*}\right)$
Re_x	Reynolds number
$Re_x^{-1/2} N u_x$	heat transfer rate
T^*	fluid temperature (K)
T_1^*	temperature on lower wall
T_2^*	temperature on upper wall
T_∞^*	fluid temperature far away from the surface
T_w^*	constant fluid temperature of the wall
τ_w	wall shear stress
(u_1, v_1)	velocity components along x^*, y^* axis
(x^*, y^*)	cartesian co-ordinate's
U_w^*	stretching velocity
U_∞^*	free stream velocity

Greek symbols

ϕ	dimensionless concentration
λ^*	ratio parameter= $\frac{b_1}{a_1}$
υ^*	kinematic viscosity= $\frac{\mu}{\rho_f}$ $(m^2 s^{-1})$
σ^*	Boltzmann constant $(wm^2 s^{-1} K^{-4})$
θ	dimensionless temperature
Γ_1, Γ_2	temperature and concentration, Biot numbers respectively
$(\upsilon^*)'$	couple stress viscosity= $\frac{n}{\rho_f}$
ρ	fluid density $(Kg.s^{-1})$
$\alpha_m{}^*$	thermal diffusivity= $\frac{k}{(\rho C)_f}$ $(m^2 s^{-1})$
$\mathrm{Sh}\,\mathrm{Re}_x^{-1/2}$	mass transfer rate
η_1	similarity variable
μ	dynamic viscosity $(Pa.s^{-1})$

Subscripts

∞	condition at free stream
w	wall mass transfer velocity

Abbreviations

HS	heat source
CSEF	couple stress Casson fluid
SS	stretching sheet
CR	chemical reaction
NNF	non-Newtonian fluid
HTR	heat transfer rate
MTR	mass transfer rate
HMTR	heat and mass transfer rate
CSF	couple stress fluid
CS	couple stress
SFC	skin friction coefficient
MF	magnetic field
BL	boundary layer
BC	boundary condition